THE DISPERSION CHARACTERISTICS OF LONGITUDINAL PLASMA OSCILLATIONS NEAR CYCLOTRON HARMONICS [+])

R.S. Harp [++])

IPP 2/43 August 1965

INSTITUT FÜR PLASMAPHYSIK

GARCHING BEI MÜNCHEN

INSTITUT FÜR PLASMAPHYSIK

GARCHING BEI MÜNCHEN

THE DISPERSION CHARACTERISTICS OF LONGITUDINAL PLASMA OSCILLATIONS NEAR CYCLOTRON HARMONICS [+])

R.S. Harp [++])

IPP 2/43 August 1965

[+]) Paper presented at the Seventh International Conference on Phenomena in Ionized Gases, Belgrade/Yugoslavia 1965.

[++]) National Science Foundation Postdoctoral Fellow (USA).

Die nachstehende Arbeit wurde im Rahmen des Vertrages zwischen dem Institut für Plasmaphysik GmbH und der Europäischen Atomgemeinschaft über die Zusammenarbeit auf dem Gebiete der Plasmaphysik durchgeführt.

IPP 2/43 R.S. Harp The Dispersion Characteristics of Longitudinal Plasma Oscillations near Cyclotron Harmonics.

August 1965 (in English).

Abstract

Interest has been recently focussed on cyclotron harmonic waves due to their importance in several fields of plasma and ionosphere physics. The observation of anomalously high r.f. radiation at harmonics of the electron cyclotron frequency in hot plasmas, as well as effects measured by topside ionospheric sounding satellites appear to be explainable in terms of cyclotron harmonic wave theory. In this paper, the theory is briefly reviewed, and computed results of the hot plasma dielectric constant and dispersion relations for the waves are presented. Experimental results are presented which for the first time clearly demonstrate transmission of the waves between cylindrical probes. A complete explanation is given of the transmission characteristics between the probes which are seen to depend on the hot plasma dielectric constant as well as the freely propagating wave modes. The use of an r.f. probe system is considered as a plasma diagnostic method whereby the magnetic field, plasma density, and electron temperature may be accurately evaluated.

1. Introduction

Treatments of a plasma in a magnetic field as a cold electron gas have been successful in explaining many phenomena, particularly in the field on ionospheric research. In recent years, however, phenomena have been observed which cannot be explained by the simplified treatment, and interest has arisen in the properties of a plasma with non-zero temperature. LANDAUER [1]) has observed microwave radiation from a plasma in narrow frequency bands centered on harmonics of the electron cyclotron frequency up to the 45^{th} harmonic. Observations from the Canadian top-side sounder Alouette [2]) indicate additional cyclotron harmonic phenomena. Electrons with a finite thermal velocity in a magnetic field gyrate with a constant frequency ω_c. Thus electric fields in the plasma at ω_c or harmonics of ω_c may synchronously couple to the motion of the electrons. This results in singularities in the plasma dielectric constant at harmonics of ω_c.

This paper presents an experimental investigation of the propagation of r.f. signals between two probes immersed in a plasma as a function of the longitudinal magnetic field imposed on the plasma. The results observed may be explained in terms of direct capacitive coupling between the probes, which exhibits singularities at harmonics of the cyclotron frequency, and a signal transmitted by longitudinal oscillation modes of the type discussed by BERNSTEIN [3]). Through measurements made at various probe spacings and plasma density, a complete comparison may be made with theory. The plan of the paper is, therefore, as follows: A brief review of theory and numerical evaluations of the dielectric constant and dispersion relation are given in section 2. Section 3 gives the experimental results where they are compared in detail with theory. Section 4 discusses possible uses of the measuring technique as a diagnostic method, whereby the parameters of a plasma may be measured with high accuracy.

2. Review of Theory

A summary of cyclotron harmonic theory is given by STIX [4]). For the special case of $k \perp B$ and $E \parallel k$ the dispersion relation for electrostatic waves becomes simply:

$$\epsilon_{xx} = 0 \quad , \tag{1}$$

where ϵ_{xx} is the dielectric tensor component in the direction of propagation given by:

$$\epsilon_{xx} = 1 - \frac{2e^{-\lambda}}{\lambda} \frac{\omega_p^2}{\omega_c^2} \sum_{n=1}^{\infty} \frac{I_n(\lambda)}{(\frac{\omega}{n\omega_c})^2 - 1} \quad . \tag{2}$$

Here ω_p, ω, ω_c are, respectively, plasma frequency, working frequency, and electron cyclotron frequency; I_n is the Bessel funtion of the first kind of imaginary argument, and $\lambda = k^2R^2$ with k the propagation constant and R the larmor radius. Eq. (2) may be readily evaluated with the aid of a computer, and the curves of Fig. 1 will prove important in understanding the experimental results to be presented. In the case of vanishing electron temperature, Eq. (2) may be expanded to first order in λ, reducing to the well known cold plasma dielectric constant:

$$\epsilon_{xx} = 1 - \frac{\omega_p^2}{\omega^2 - \omega_c^2} \quad . \tag{3}$$

Modifications to the dielectric constant introduced by the finite electron temperature are the discontinuities at the various cyclotron harmonics. These increase in amplitude with λ and ω_p/ω; decreasing at higher values of ω/ω_c. The average value of the curves, however, follows Eq. (3), passing through zero when:

$$\omega^2 = \omega_H^2 = \omega_p^2 + \omega_c^2 \quad , \tag{4}$$

where ω_H is the upper hybrid frequency.

Solutions of Eq. (1) are given by CRAWFORD [5]) for the case ω_p/ω_c = const. In our experiments, however, the working frequency and plasma frequency are constant, so solutions with ω_p/ω = const. are considered. These are given in Fig. 2 for a range of parameters. The characteristics of the curves

are sharply divided depending on the relationship between ω and ω_H. For frequencies above the hybrid frequency, the dispersion relation consists of transmission bands adjoining the harmonics. Below the hybrid frequency, however, transmission is obtained for all frequencies.

3. Experimental Results

3.1. Description of the apparatus

The experimental apparatus as sketched in Fig. 3 consists of a cross-shaped glass vacuum enclosure having six identical arms with an inner diameter of 7.5 cm. Through the lower arm, the system is continuously pumped by an oil diffusion pump. Argon is introduced into the system by means of a leak valve. Typical operating pressures range from 3×10^{-4} torr to 1×10^{-2} torr. A magnetic field is provided by a pair of Helmholtz coils 54 cm in diameter. The magnetic field is homogeneous to better than 1 % over the probe region, and to about 20 % over the entire discharge. The field current may be slowly swept by means of a motor-driven autotransformer covering its full range in approximately 6 minutes. The discharge anode consists of a stainless-steel disk, and the cathode is constructed of four oxide-coated nickel mesh strips having a total emitting area of 4 x 4 cm. At an argon pressure of 3×10^{-4} torr a discharge may be produced with anode currents of from 1 milliamp to 10 amps with an anode potential of approximately 20 volts. At high magnetic fields, the discharge is confined to a 4 x 4 cm cylinder formed by the cathode, and the plasma density is essentially independent of the magnetic field, while for fields lower than 30 gauss the discharge rapidly expands to fill the discharge chamber, and the plasma density is correspondingly reduced.

Through two remaining sidearms, r.f. probes are inserted into the plasma column. They consist of 0.3 mm wires 5 cm long lying parallel to the magnetic field. A sketch appears in Fig. 4. 50 ohm coaxial lines connect the probes to external equipment. The probes may be accurately positioned radially by means of a lead screw, with the position being read on a

dial indicator to 0.01 mm. A bellows arrangement allows the probes to be positioned in the same horizontal plane. Experience has shown that inaccuracy in the probe alignment of more than 1 degree either between the probes or relative to the magnetic field causes degradations of the experimental results.

3.2. Measurements of the transmitted signal amplitude

The r.f. signal transmitted through the plasma was measured with the arrangement shown in Fig. 3. An 800 Mc signal modulated at 1000 cps was applied to one of the probes after being attenuated to a low level of approximately -15 dbm. The transmitted signal was then amplified and detected by the superheterodyne receiver, which includes a narrow-band 1000 cps amplifier. The detected output signal proportional to the transmitted power drove the y-input of an x-y recorder. A voltage proportional to the magnetic field drove the x-input of the recorder.

By virtue of the narrow-band 1000 cps amplifier, the receiver is sensitive only to signals modulated with 1000 cps. Thus any noise signals generated in the plasma do not cause a deflection of the recorder.

The transmitted signals vs. magnetic field are shown in Figs. 5a to 5e for discharge currents from 10 to 600 milliamps. Since the magnetic field is proportional to ω_c/ω, the harmonics of the cyclotron frequency occur at values 0.5, 0.33, 0.25, etc. Probe spacing for the curves is 1.2 cm. Receiver gain was adjusted from curve to curve to give a reasonably constant dynamic range. The zero signal level is indicated for each curve by the reference line under the letter H. Compared to transmission without plasma, the curves represent a range from -30 db to +10 db.

At low currents we find the transmission has abrupt discontinuities at harmonics of the cyclotron frequency. At currents above 80 milliamps, we notice the appearance of wave patterns above the harmonics. On all curves, we observe a minimum of transmission labelled by the letter H which traverses the

range of magnetic field as the discharge current is varied. At currents above 125 milliamps the sharp discontinuities at the harmonics become rounded and displaced to lower values of magnetic fields. Such peaks have also been observed by CRAWFORD in a mercury vapor discharge under similar conditions of plasma density, probe geometry, and probe spacing. At other probe spacings, the only essential change observed in the curves is in the periodicity of the wave patterns. These measurements were made at a pressure of 3×10^{-4} torr in argon. At higher pressures the amplitude of the wave patterns was observed to decrease, particularly for the higher harmonics, until at a pressure of 3×10^{-3} torr they were not clearly distinguishable.

At frequencies other than 800 Mc, the features of the curves remain essentially unchanged, aside from the expected scaling of magnetic field and probe spacing. At a frequency of 1600 Mc peaks at the harmonics have been measured up to the 35^{th} harmonic.

3.3. Quasi-static model of the probe system

The response of a plasma to an externally applied electric field is characterized by solutions of the inhomogeneous equation $D/E = \epsilon(\omega,k)$. The complete response, however, also contains solutions of the homogeneous equation $0 = \epsilon(\omega,k)$. Considering at first solutions of the inhomogeneous equation, a quasi-static model will be developed which will prove useful in understanding the transmission curves of Figs. 5a to 5e. Fig. 4a shows the probe system, and a sketch of the r.f. electric field distribution under appropriate excitation of the probes. The dimensions involved are much less than the free space wavelength at 800 Mc, and hence the field distribution is essentially a static one. From a circuit point of view, the field lines from one probe to the other may be represented by a capacitance between them as shown in Fig. 4b, and the field lines from each probe to the transmission-line shield may be represented by a capacitance to ground. The dielectric of the capacitors is assumed to have the same properties as that of the plasma, i.e. $D/E = \epsilon(\omega,k)$.

Let us consider the transmission of signals from sender to receiver under these varying conditions, as shown in Fig. 6. When $|\epsilon|$ is very small, the impedance of C_1, C_2, C_3 is very large and there is no transmission as shown in Fig. 6b. As $|\epsilon|$ increases, the transmission is at first proportional to the increasing admittance of C_1. At larger values of ϵ, more and more current is shunted to ground through C_2 and C_3. There is thus a maximum in transmission when the capacitors are comparable in impedance to the 50 ohm transmission line. At higher values of ϵ, C_2 and C_3 progressively load the transmission lines resulting in a decrease of the transmitted signal. In the limit of $|\epsilon| \to \infty$ the capacitors form a short circuit, resulting in no transmission as shown in Fig. 6c. The behavior of the transmission over the range of ϵ is shown in Fig. 6a, where ϵ_m denotes the value for maximum transmission.

There are some aspects of the actual system which are neglected in the quasi-static model. The plasma density is not constant over the column and falls off rather rapidly in the vicinity of the transmission lines. The effect of a sheath at the probe is neglected. The ends of the transmission lines are covered with glass to make them vacuum-tight and, therefore, the capacitance of the probes to ground is not strictly proportional to the plasma dielectric constant. The actual system is three-dimensional, and since the plasma dielectric constant is a tensor quantity, the exact problem is more complicated. Due to these shortcomings, the true relationships of the quantitative values may differ from those of the model, but the basic description of Fig. 6 remains unchanged: the transmitted signal reaches a maximum for some value of the dielectric constant.

In addition to the homogeneous solutions, electrons reflected in the sheath surrounding the sender probe experience a transient r.f. deflecting force. The motion of the particles after this transient is represented by solutions of the homogeneous equation $\epsilon(\omega,k) = 0$. As we have seen in section 2, these solutions represent, in general, waves. To complete the explana-

tion of the observed phenomena, a superposition of the two effects must be considered.

The r.f. potential at the receiver probe given by the voltage across C_2 in the equivalent circuit is essentially constant in phase, varying in amplitude with changes in the dielectric constant.

The wave solutions are characterized by an r.f. space potential periodic with distance from the sender probe.

In Fig. 7a the r.f. potential at the receiving probe given by the quasi-static model is represented by the vector A in the phasor diagram, while the wave potential is represented by vector B. The total potential is thus the vector sum of the two. The receiver system responds to the magnitude of the sum. As the magnetic field is varied, the wavelength of the wave solutions varies, and hence the vector B rotates about A. The resulting interference pattern is diagrammed in Fig. 7b.

Having introduced the quasi-static model, we may return to the experimental results (Figs. 5a to 5e) and make a more meaningful comparison with theory. In Fig. 5a, the dielectric constant is, in general, small, and hence the transmission is proportional to ϵ. These curves correspond to $\omega_p^2/\omega^2 < 0.5$, and the identical behavior is observed as in Fig. 1 with discontinuous behavior at the harmonics, and a minimum transmission at what should be the hybrid frequency H. At higher discharge currents, the average transmission decreases, while the discontinuities at the harmonics increase. The experimental results deviate from theory in that the discontinuities are not infinitely sharp; this is probably the result of collisional damping. As the point H passes through the various harmonics as in Fig. 5c, we observe the appearance of interference patterns adjacent to the harmonics. This is associated with a basic change in the dispersion relation, as illustrated in Fig. 2, resulting in continuous transmission bands of high group velocity between harmonics.

From the relationship at the point H given by Eq. (4) may be obtained:

$$\frac{\omega_c^2}{\omega^2} = 1 - \frac{\omega_p^2}{\omega^2} \quad . \qquad (5)$$

In a positive column discharge the density and hence ω_p^2/ω^2 is proportional to discharge current. Thus plotting ω_c^2/ω^2 at point H vs. discharge current should give a straight-line relationship. This is illustrated in Fig. 8. The current for $\omega_c^2/\omega^2 = 0$ is that for $\omega_p^2 = \omega^2$. This agrees within experimental uncertainty with Langmuir probe density measurements.

At higher discharge currents the plasma dielectric constant assumes a large negative value. The transmission peaks observed at the cyclotron harmonics become rounded and displaced toward higher harmonics. This phenomenon has also been observed by CRAWFORD. It is simply a result of the plasma dielectric constant exceeding ϵ_m as described in Fig. 6a. The reason for the displacement to higher harmonics may be most easily understood by referring to Fig. 1, where ϵ is diagrammed for several values of plasma density. Let us assume, for graphic purposes, that the value of ϵ_m is -1; thus the intersection of the dielectric constant curve and the $\epsilon = -1$ curve represents the peak in transmission. As the discharge current increases, resulting in larger values of ω_p^2/ω^2, the peak in transmission is displaced to the next higher harmonic.

One point that has been neglected is the reason for giving λ a non-zero value. The explanation lies in the actual field distribution surrounding the probes which will have a dependence on distance from the probe as shown schematically in Fig. 4a. Such a distribution may be Fourier-analyzed in terms of spatial wave components of the form e^{-ikx}. The resulting transform will contain components lying in the range of approximately $k = 3\ cm^{-1}$ and $300\ cm^{-1}$. The first value represents wave components of dimensions comparable to the spacing between the probes and the second value is representative of the sheath thickness. The latter results from the rapid variation in field strength near the probes due to the cylindrical geometry. If we take a geometric average value of 30, the resulting λ at the second harmonic in our experiment is $\lambda = k^2R^2 \approx 1$ which compares with the value $\lambda = 0.5$ of Fig. 1. It should be noted, however, that in the experiments, R, the gyroradius, increases with increasing

harmonic number (smaller magnetic field) and hence λ increases quadratically with ω/ω_c. This has the effect of enhancing the dielectric constant singularities at higher harmonics as compared to the theoretical curves where the singularities rapidly diminish in magnitude.

3.4. The dispersion relation of cyclotron harmonic waves

From measurements made at various probe spacings as in Fig. 9 may be obtained the wavelength of the oscillations as a function of the magnetic field. The positions of the peaks and valleys in the interference patterns of Fig. 9 may be replotted as in the upper half of Fig. 10. The probe spacing is given by X, and an upward line represents a peak, and a downward line a valley. Intermediate curves have been included. Smooth curves are shown connecting the various points as their position varies with probe spacing. A line drawn at a constant value of ω_c/ω must intersect the maxima curves at equally spaced intervals equal to the wavelength of the plasma waves (not the half wavelength as with a standing wave). As an aid in this visualization, it may be realized that the same information contained in Fig. 10 could be obtained by holding ω/ω_c constant at specific values and varying the probe spacing; the received signal would then be maximum at points one wavelength apart. The wavelength thus obtained by measurements over a number of wavelengths is plotted in the lower half of the figure.

From a number of such constructions at various discharge currents may be obtained the dispersion relations for the waves as shown in Figs. 11a to 11c. The experimental results are compared to solutions of Eq. (1). The agreement between experiment and theory is for the most part very good, especially in Fig. 11c. In evaluating the experimental results, Langmuir probe measurements of T_e = 3.0 ev and $n_e = 8 \times 10^9$ cm^{-3} at 110 milliamps have been used.

4. Conclusions

We have seen that the quasi-static model of the probe system is capable of explaining the essential features of the transmission curves. It is interesting to speculate on the use of

such a system as a plasma diagnostic. Assuming that a plasma frequency in the range of the working frequency is obtainable, as for example with the curves of Fig. 5b, the point at which ω_c/ω may be measured with extremely good accuracy from the position of the peak. In our curves the sharpness of the peak permits this point to be located to about 0.5 % accuracy. Since the working frequency may be measured accurately with a digital frequency counter, it is possible to calibrate the magnetic field in this manner. In addition, from the location of the point H of minimum transmission at which $\omega = \sqrt{\omega_p^2 + \omega_c^2}$ we may obtain the plasma frequency, since the other quantities are known. Finally, from measurements of the wavelength of the cyclotron harmonic waves, we can obtain the larmor radius, and hence the electron temperature. It must be borne in mind, however, that the method is probably limited to the UHF range of frequencies. Above 1 to 2 kMc, the free space wavelength of the working frequency becomes quite short, and unless the probes are scaled proportionately, the quasi-static model of the probe system is no longer valid.

Acknowledgement

Useful discussions of the work with Dr. G. Müller are gratefully acknowledged, as is the work of R. Moser and W. Bitter in preparing the apparatus. The theoretical curves in the last three figures were supplied by Drs. G. Kino and F.W. Crawford.

This work has been undertaken as part of the joint research program of the Institut für Plasmaphysik and EURATOM.

References

1) G. Landauer, Proc. Fifth Int. Conf. on Ioniz. Phen. in Gases, Munich, Germany, July 1961 (North Holland Publishing Co., Amsterdam), I, 389; J. Nucl. Energy Part C 4, 395 (1962); Bull. Am. Phys. Soc. 9, 312 (1964).

2) G.E.K. Lockwood, Can. J. Phys. 41, 190 (1963).

3) I.B. Bernstein, Phys. Rev. 109, 10 (1958).

4) T.H. Stix, The Theory of Plasma Waves (McGraw-Hill Book Co., New York 1962), 1st Ed., Chapters 8 and 9.

5) F.W. Crawford, G.S. Kino, and H.H. Weiss, Phys. Rev. Lett. 13, 229 (1964); Microwave Lab. Rep. No. 1210, Stanford University (August 1964).

Figure Captions

Fig. 1 The plasma dielectric constant ϵ vs. ω/ω_c for various values of ω_p^2/ω^2 at a constant value of $\lambda = 0.5$.

Fig. 2 The dispersion relation for the electrostatic modes for various values of ω_p^2/ω^2. R is the electron gyroradius, k the propagation constant, and ω_c the cyclotron frequency.

Fig. 3 Experimental arrangement for measurement of r.f. transmission vs. magnetic field.

Fig. 4 The r.f. probe system and its quasi-static equivalent circuit.

Fig. 5a Measurements of the transmitted r.f. signal vs. magnetic field at a constant frequency. Curves for different discharge currents are displaced for clarity; zero transmission is indicated by the line under point H.

Fig. 5b Of interest here are the abrupt discontinuities at harmonics of the electron cyclotron frequency ($\omega_c/\omega = 0.5, 0.35, 0.25 \ldots$).

Fig. 5c Of interest here is the onset of interference patterns adjacent to the cyclotron frequency harmonics as the hybrid frequency (point H) passes through the harmonics.

Fig. 5d The peaks at the harmonics become progressively rounded and displaced toward higher harmonics (lower magnetic field) with increasing discharge current.

Fig. 5e Further displacement of the peaks. At values of ω_c/ω less than 0.1 the plasma density rapidly decreases due to lack of confinement of the column.

Fig. 6 The quasi-static probe model and the resulting relation between plasma dielectric constant and transmission.

Fig. 7 The combination of a capacitively transmitted signal of constant phase with a wave-transmitted signal whose phase varies rapidly with magnetic field results in interference patterns.

Fig. 8 The relationship between the transmission minimum at point H and discharge current.

Fig. 9 Transmission vs. magnetic field at various probe spacings with a discharge current of 400 milliamps.

Fig. 10 The method of obtaining the wavelength λ (bottom curves) from the interference patterns of Fig. 9. An upward stroke represents a peak, a downward stroke a valley, while X is the probe spacing.

Fig. 11a Experimental dispersion curves compared with theory between the third and fourth harmonic.

Fig. 11b Experimental dispersion curves compared with theory between the second and third harmonic.

Fig. 11c Experimental dispersion curves compared with theory between the first and second harmonic.

Figure 1

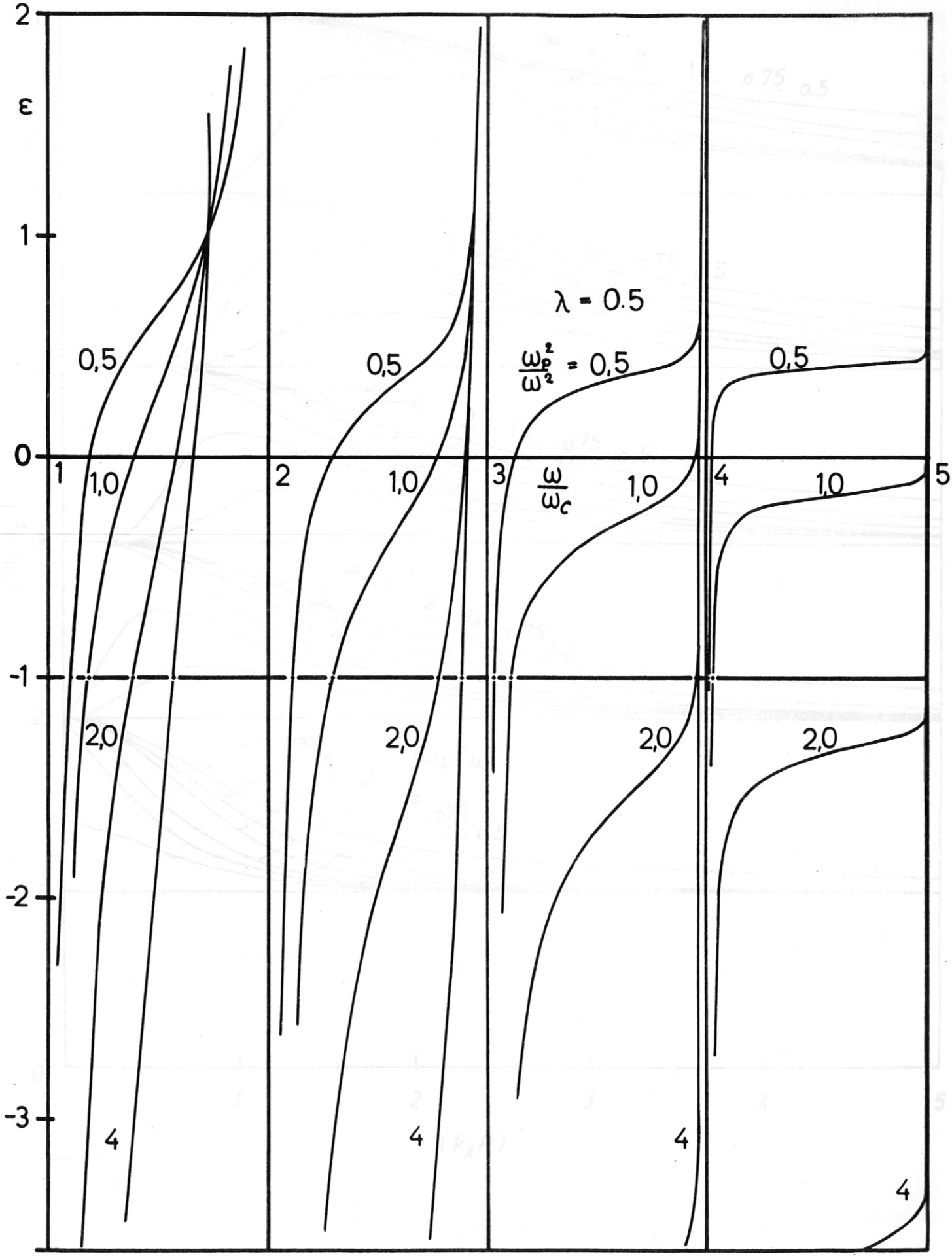
2
ε
1
0
-1
-2
-3
λ = 0.5
$\frac{\omega_p^2}{\omega^2}$ = 0,5
0,5
1,0
2,0
4
1
2
3
4
5
$\frac{\omega}{\omega_c}$

Figure 2

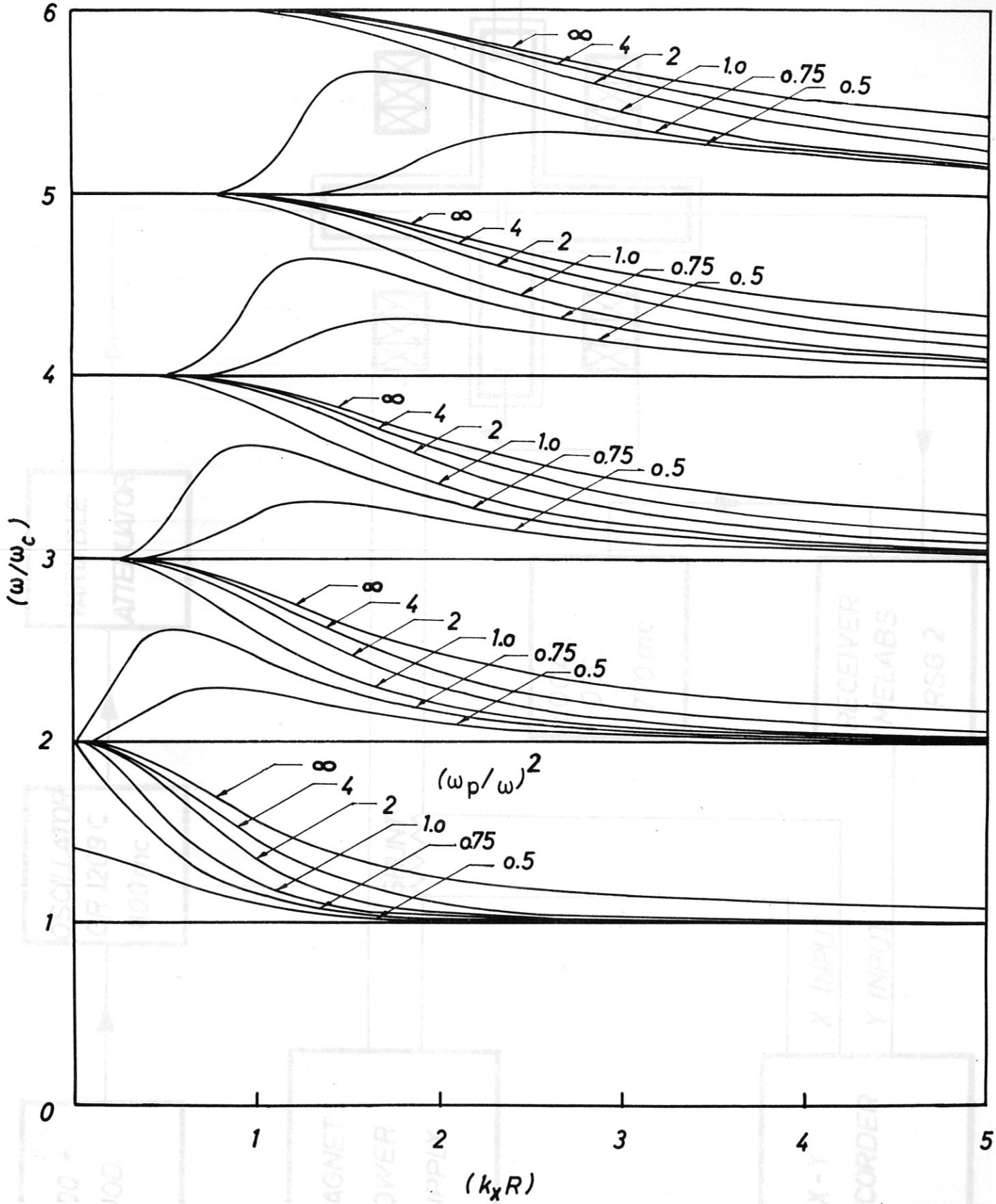

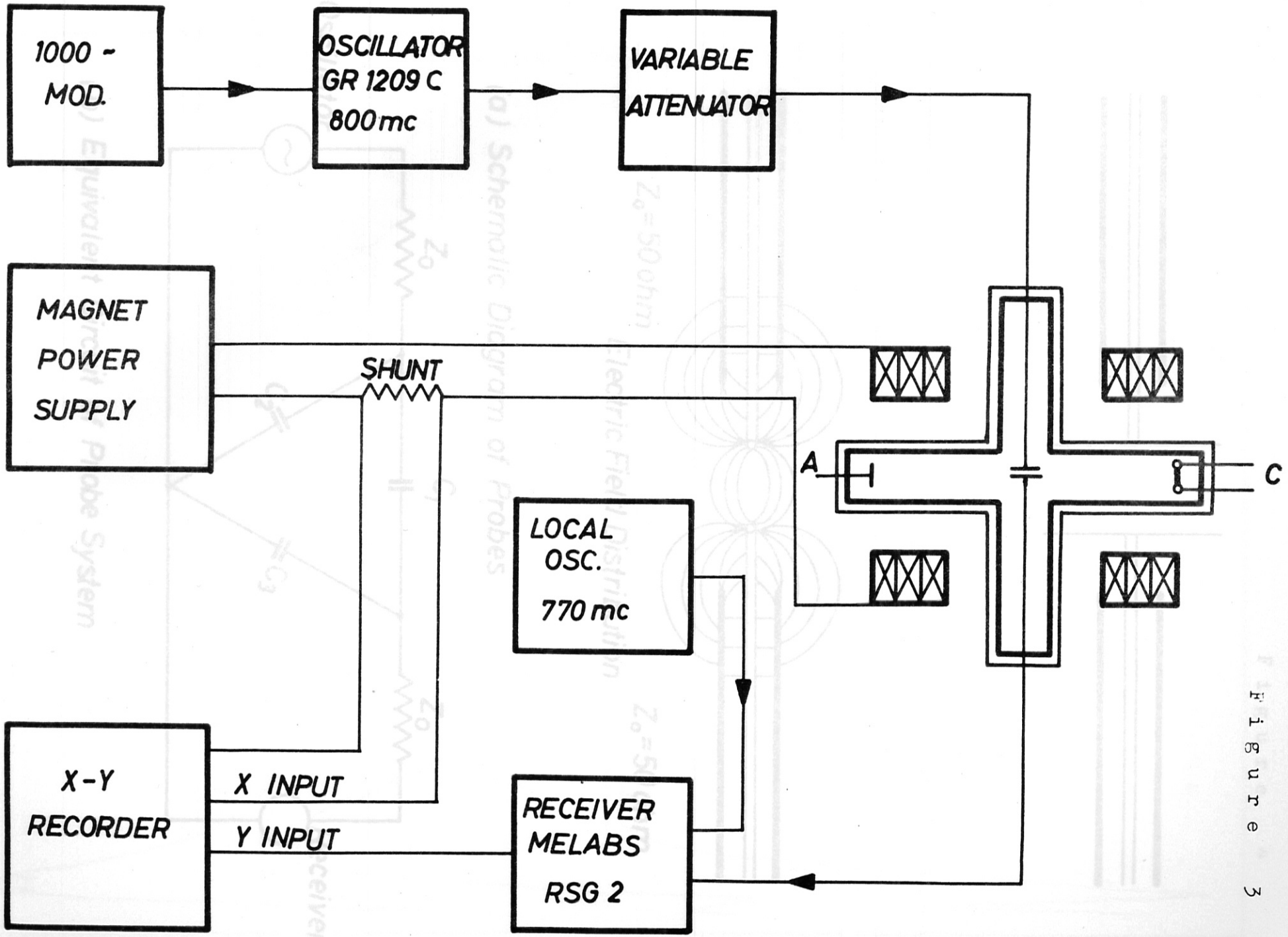
1000 - MOD.
OSCILLATOR GR 1209 C 800 mc
VARIABLE ATTENUATOR
MAGNET POWER SUPPLY
SHUNT
A
C
LOCAL OSC. 770 mc
X-Y RECORDER
X INPUT
Y INPUT
RECEIVER MELABS RSG 2

Figure 3

Figure 4

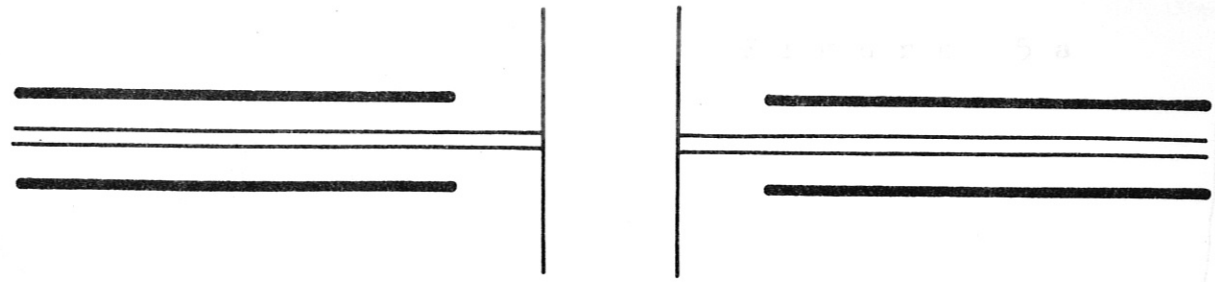

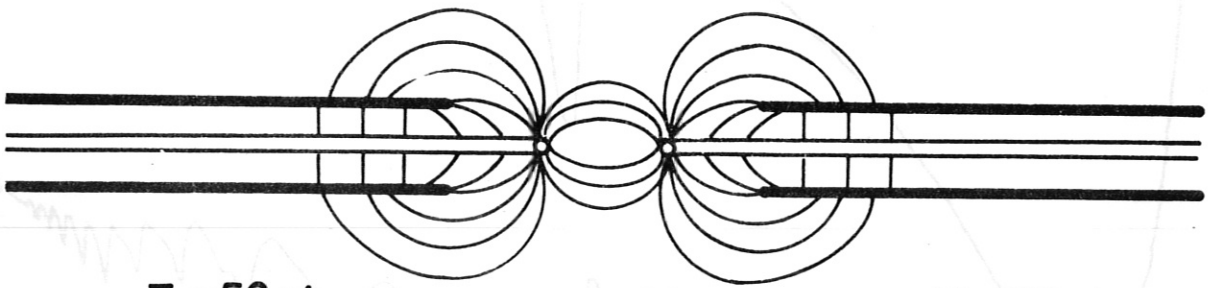

Z_o=50 ohm Z_o=50 ohm

Electric Field Distribution

(a) Schematic Diagram of Probes

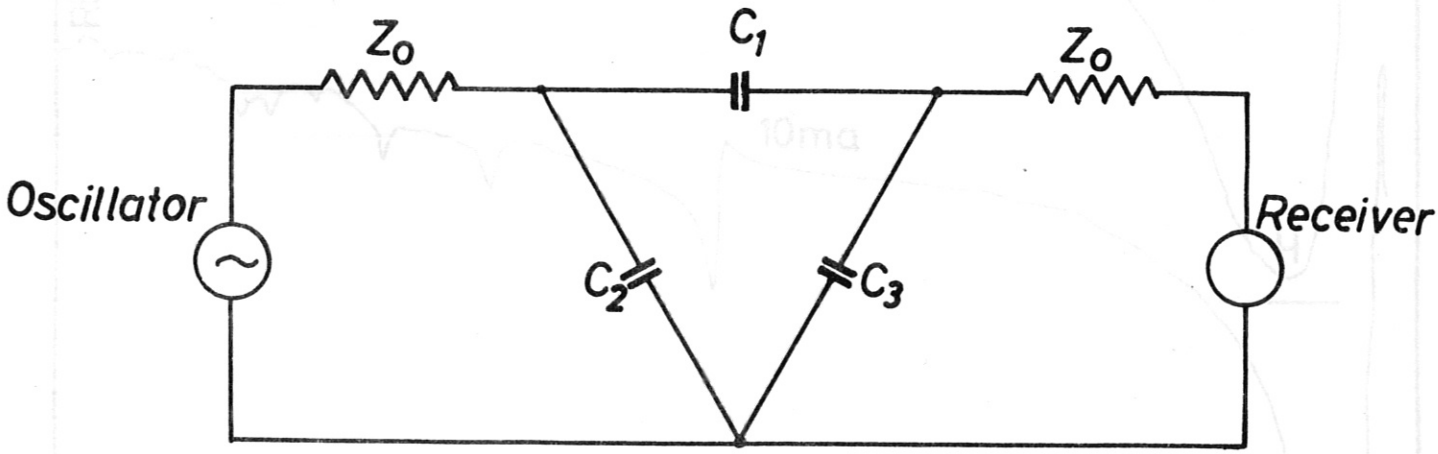

(b) Equivalent Circuit of Probe System

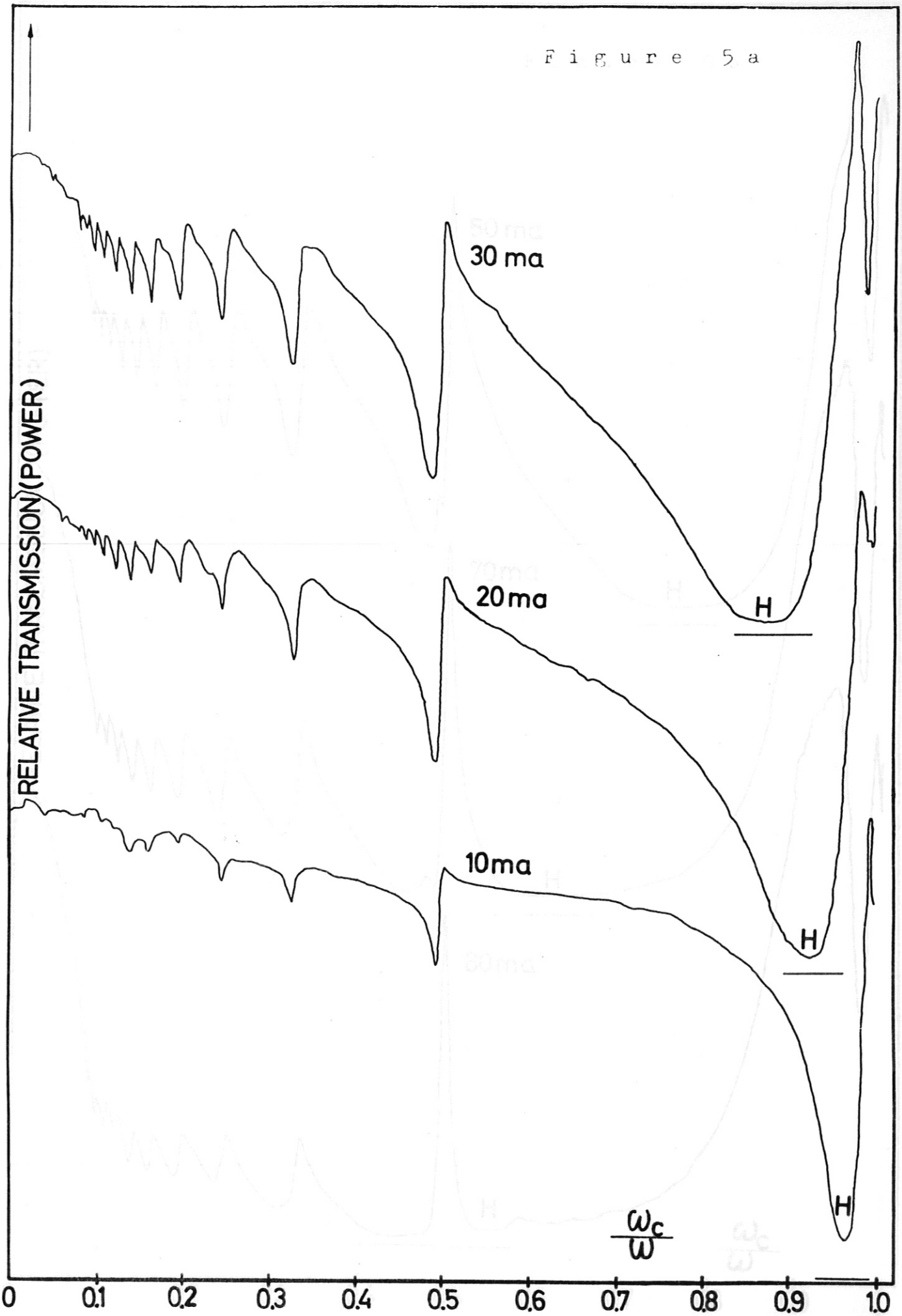
Figure 5a
30 ma
20ma
10ma
H
H
H
RELATIVE TRANSMISSION (POWER)
$\frac{\omega_c}{\omega}$
0
0.1
0.2
0.3
0.4
0.5
0.6
0.7
0.8
0.9
1.0

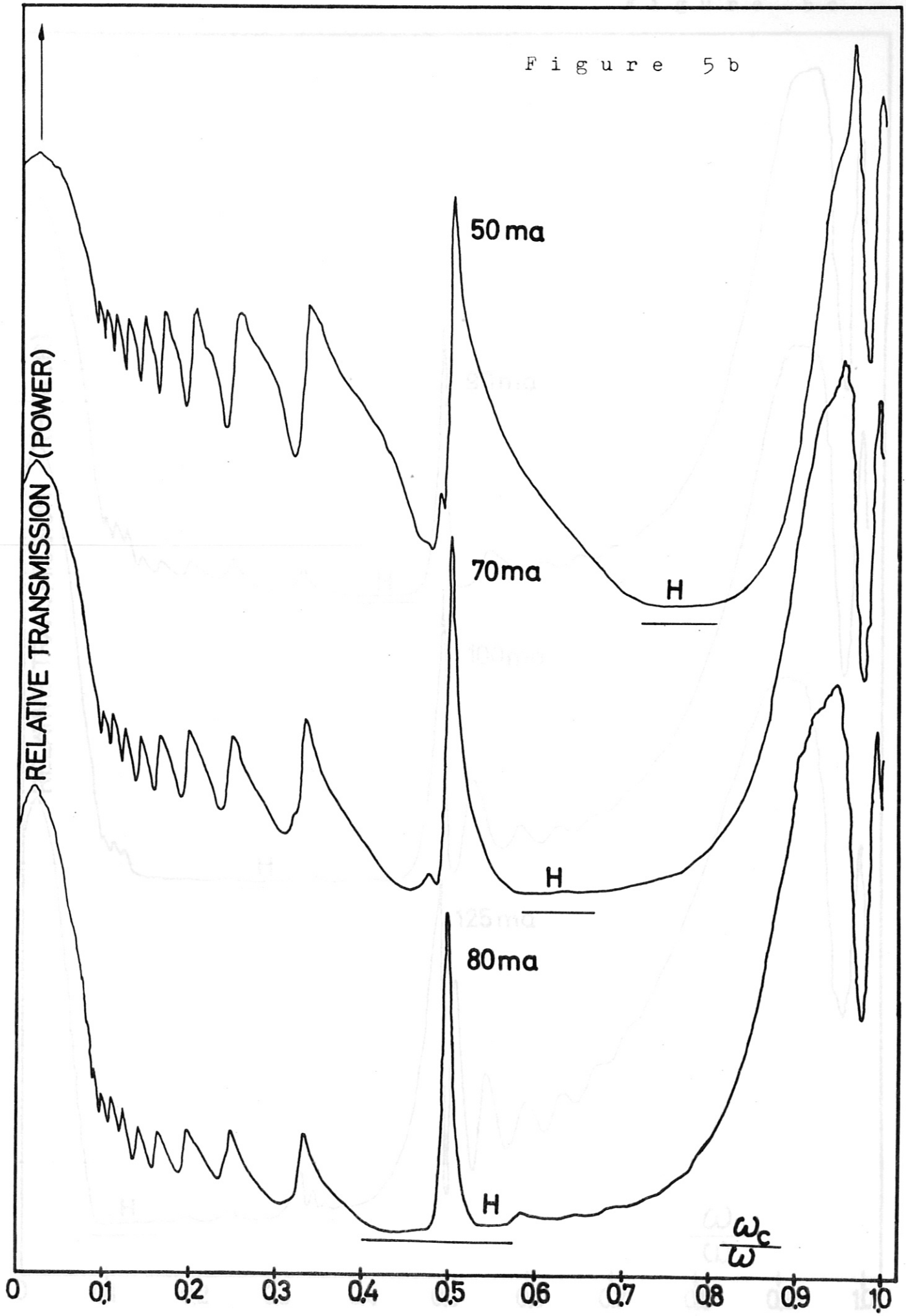
Figure 5b
RELATIVE TRANSMISSION (POWER)
50 ma
70ma
80ma
H
H
H
0
0.1
0.2
0.3
0.4
0.5
0.6
0.7
0.8
0.9
1.0
ωc/ω

Figure 5c

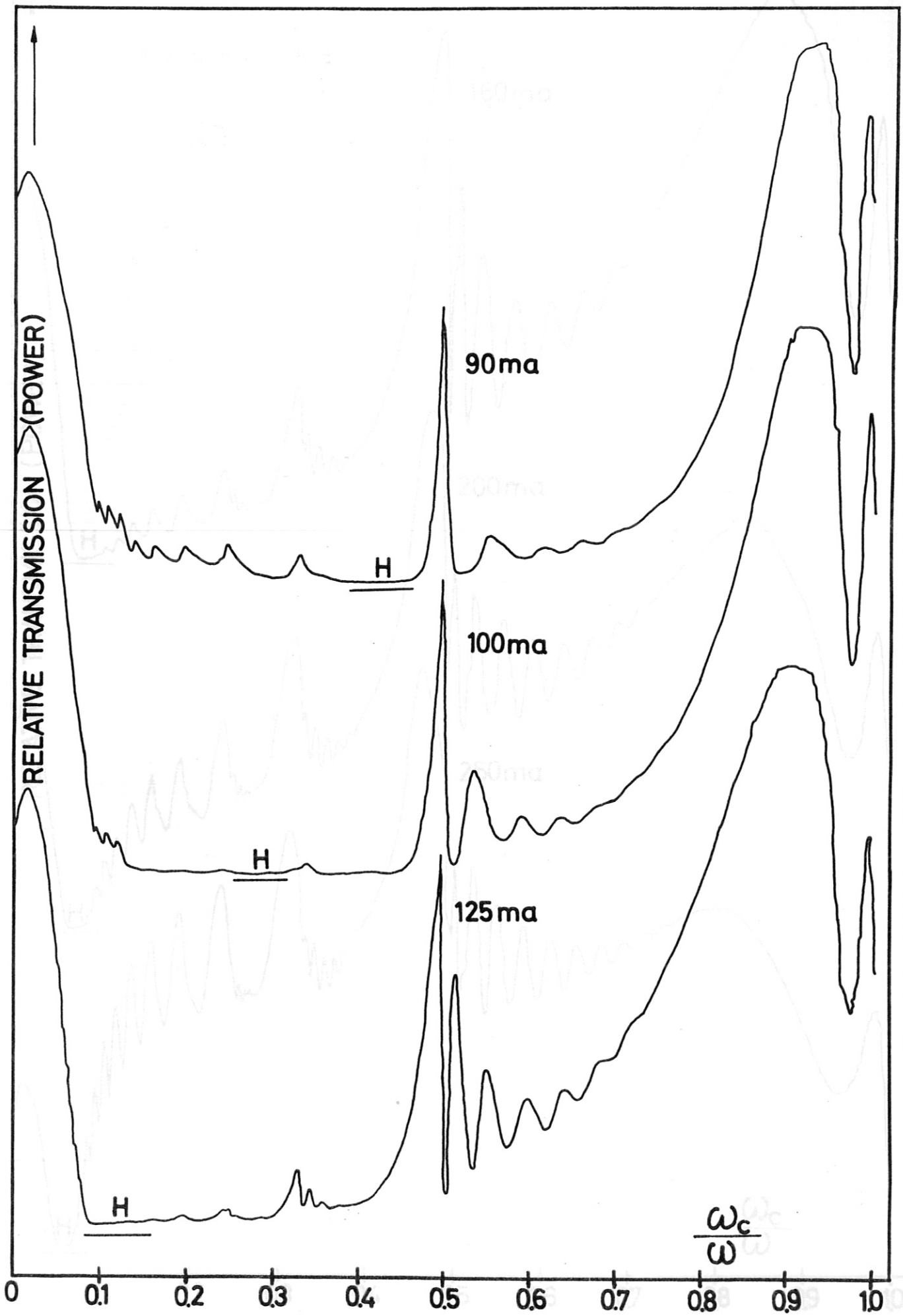
RELATIVE TRANSMISSION (POWER)
90ma
100ma
125ma
H
H
H
$\frac{\omega_c}{\omega}$
0
0.1
0.2
0.3
0.4
0.5
0.6
0.7
0.8
0.9
1.0

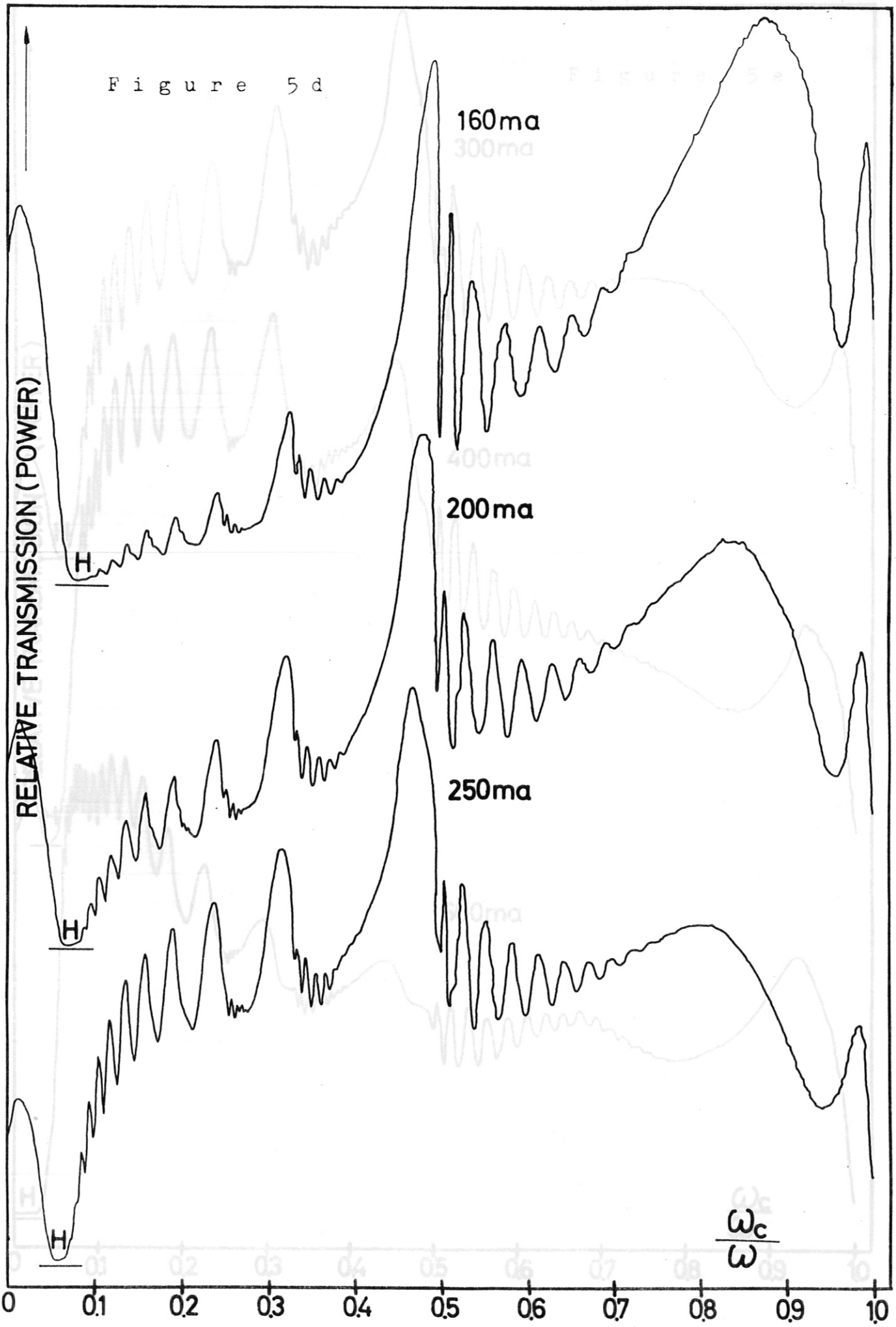
Figure 5d
160ma
200ma
250ma
H
H
H
RELATIVE TRANSMISSION (POWER)
$\frac{\omega_c}{\omega}$
0
0.1
0.2
0.3
0.4
0.5
0.6
0.7
0.8
0.9
1.0

160ma
200ma
250ma
H
H
H
RELATIVE TRANSMISSION (POWER)
$\frac{\omega_c}{\omega}$
0
0.1
0.2
0.3
0.4
0.5
0.6
0.7
0.8
0.9
1.0

Figure 5e

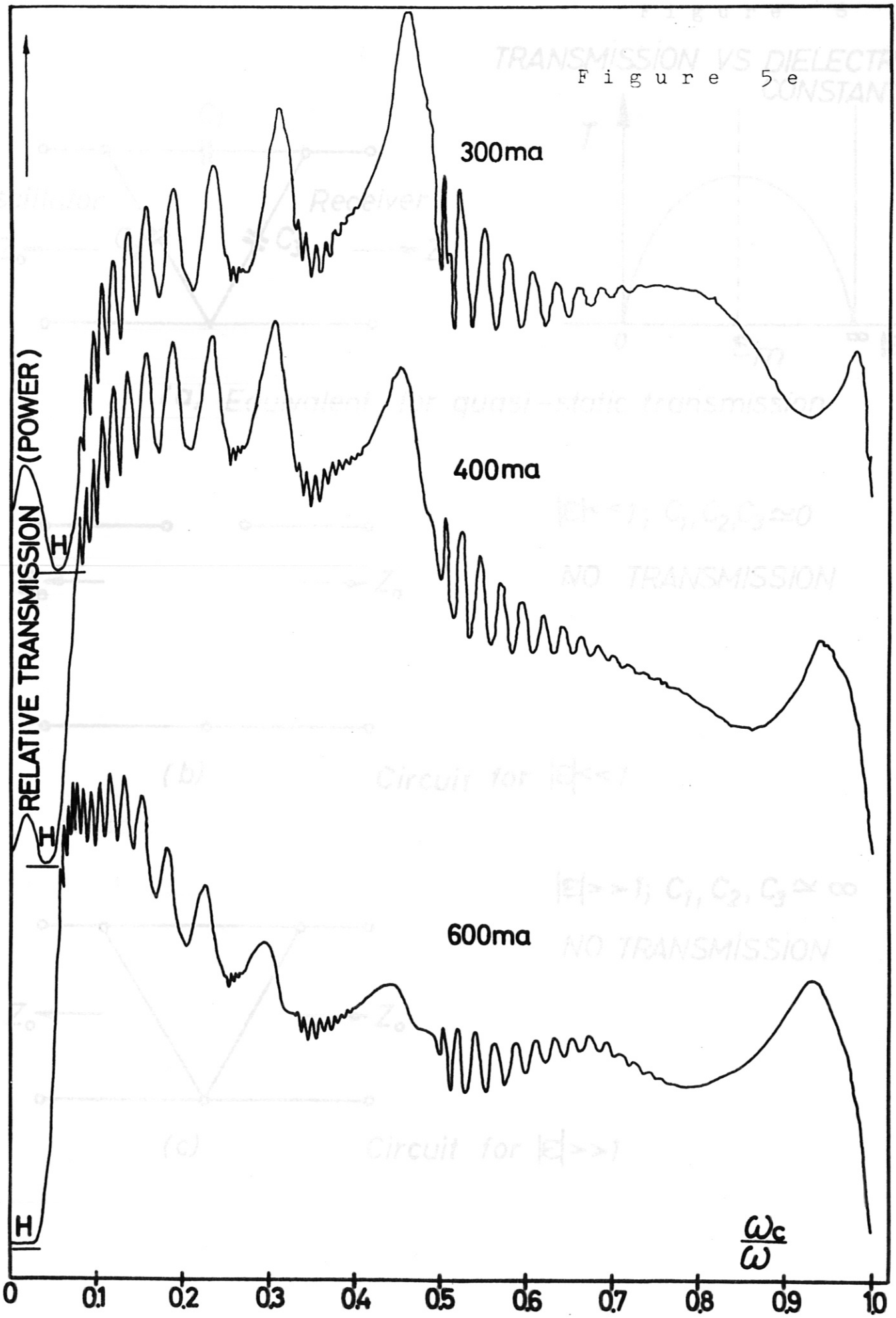
300ma
400ma
600ma
RELATIVE TRANSMISSION (POWER)
H
H
H
0
0.1
0.2
0.3
0.4
0.5
0.6
0.7
0.8
0.9
1.0
ωc/ω

Figure 6

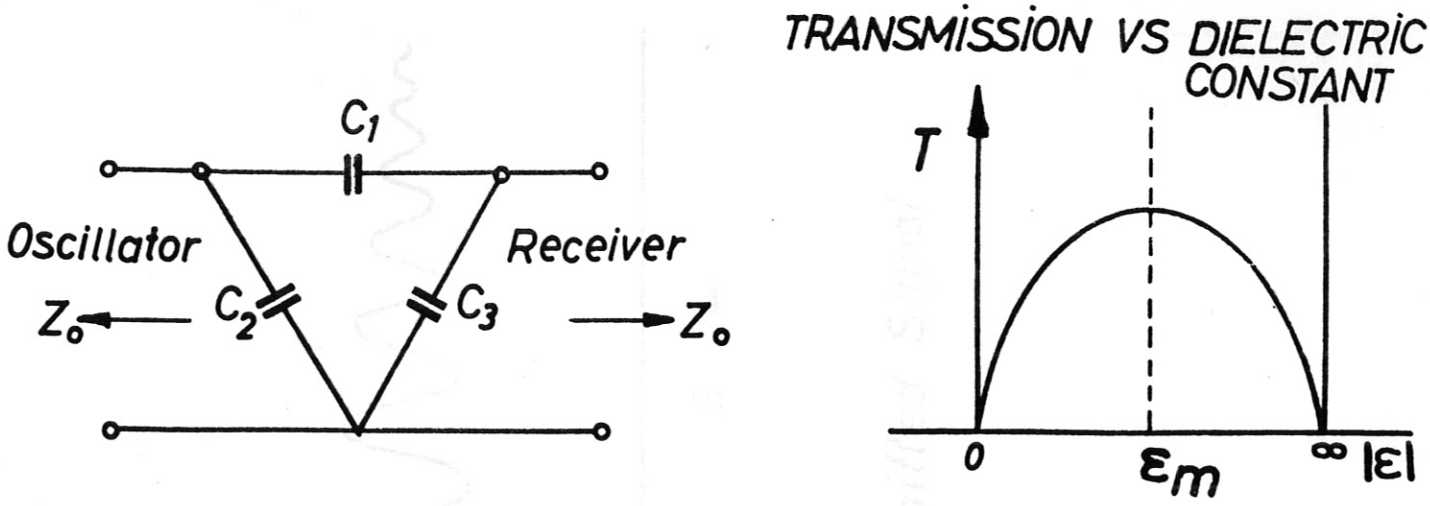

(a) Equivalent for quasi-static transmission

$|\varepsilon| << 1$; $C_1, C_2, C_3 \simeq 0$

NO TRANSMISSION

(b) Circuit for $|\varepsilon| << 1$

$|\varepsilon| >> 1$; $C_1, C_2, C_3 \simeq \infty$

NO TRANSMISSION

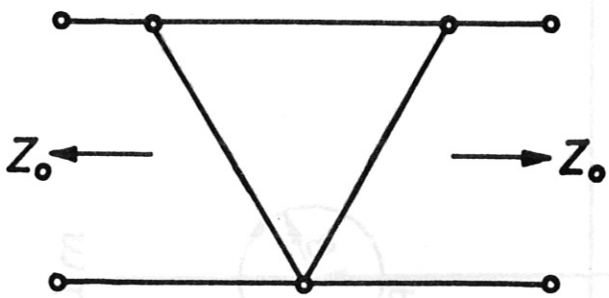

(c) Circuit for $|\varepsilon| >> 1$

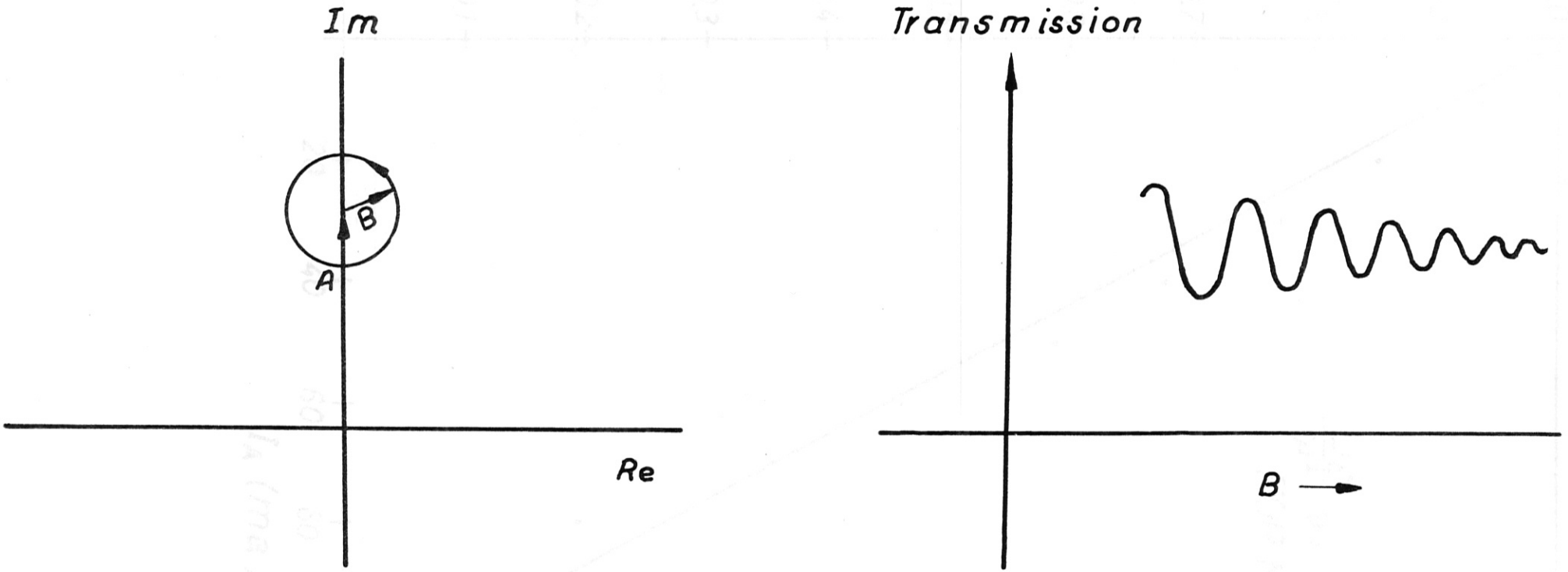

(a) Phasors at Receiver Probe (b) Transmitted Signal

Figure 7

Figure 8

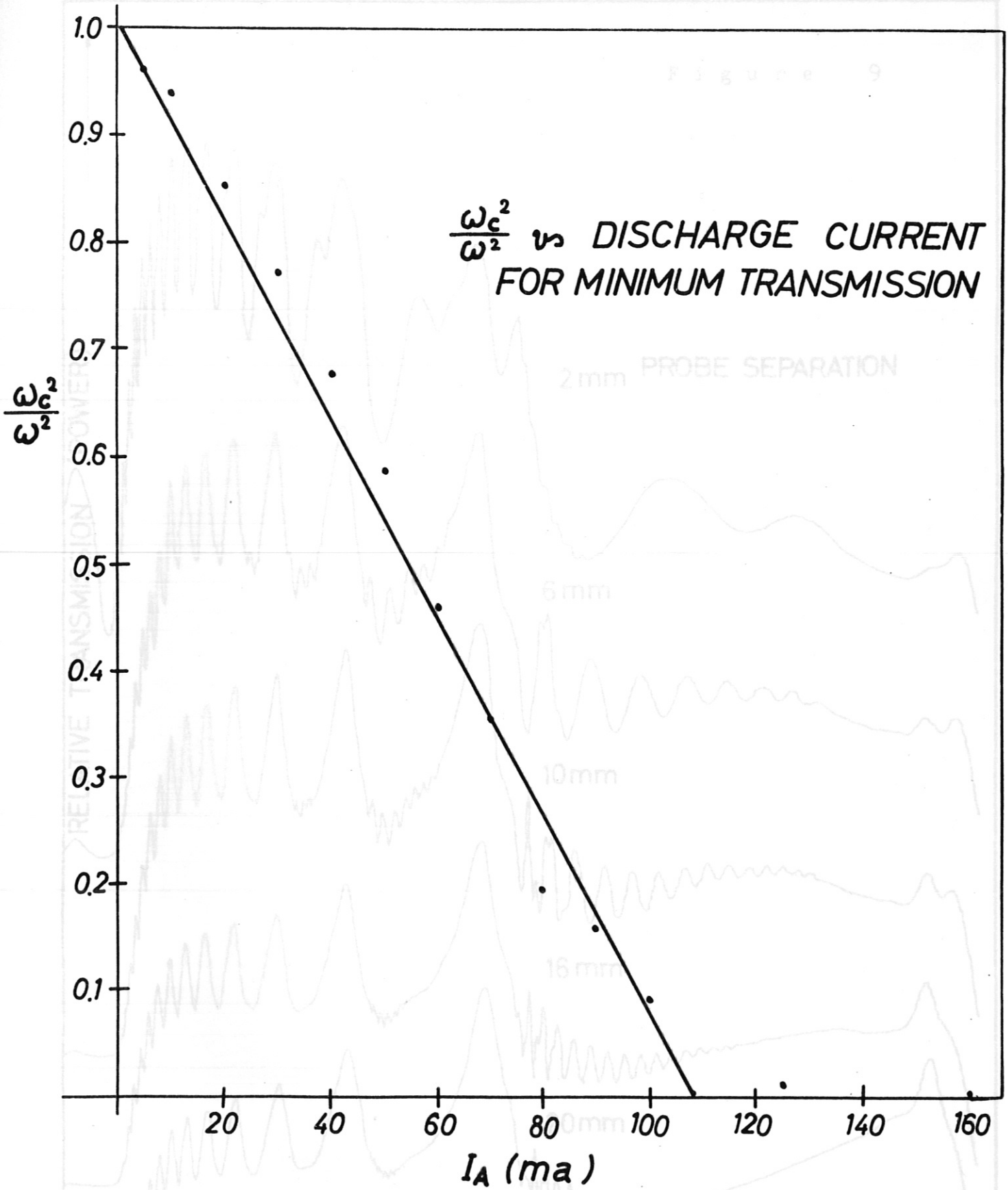
$\frac{\omega_c^2}{\omega^2}$ vs DISCHARGE CURRENT FOR MINIMUM TRANSMISSION
$\frac{\omega_c^2}{\omega^2}$
1.0
0.9
0.8
0.7
0.6
0.5
0.4
0.3
0.2
0.1
20
40
60
80
100
120
140
160
I_A (ma)

Figure 9

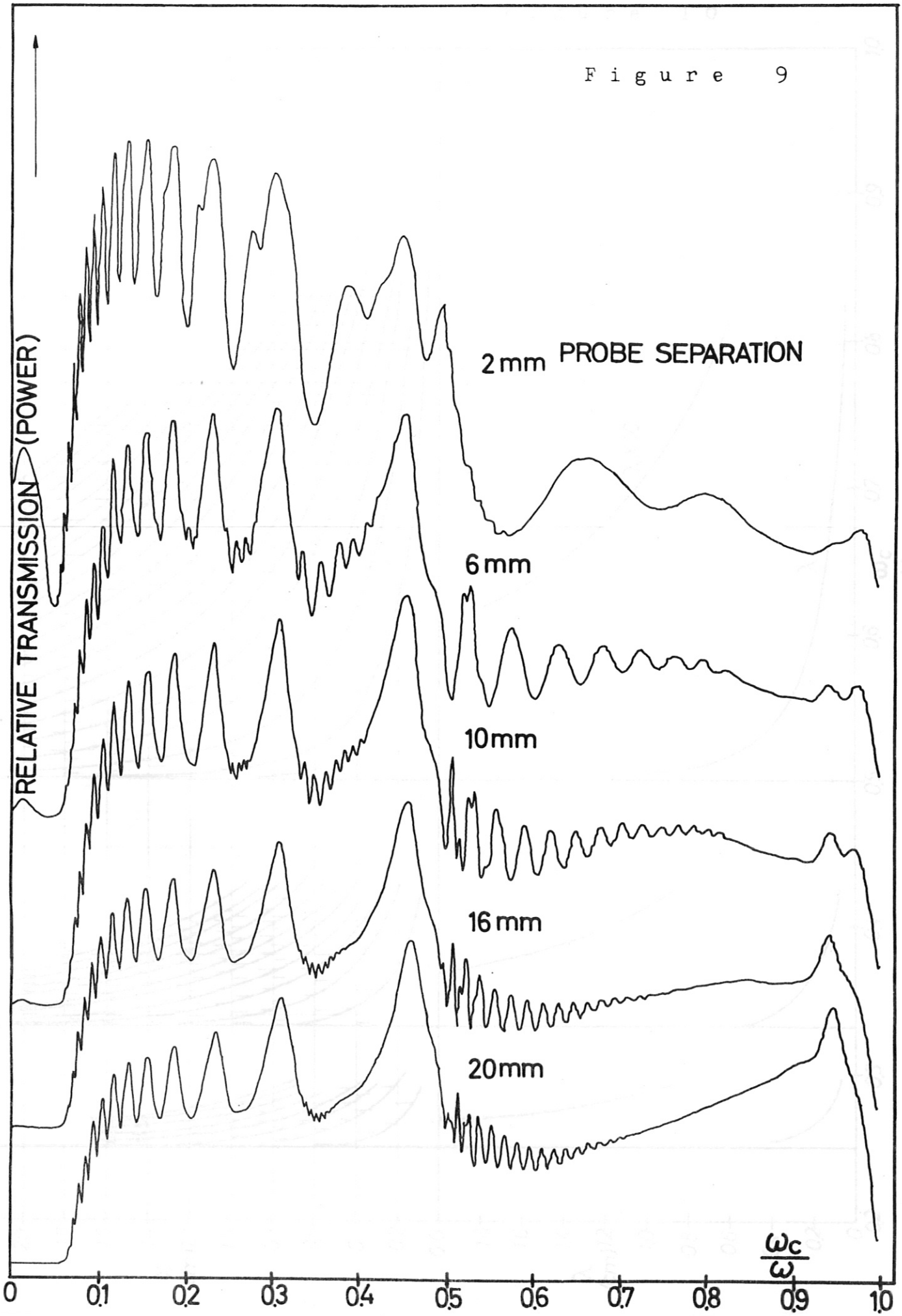
RELATIVE TRANSMISSION (POWER)
2mm PROBE SEPARATION
6mm
10mm
16mm
20mm
0
0.1
0.2
0.3
0.4
0.5
0.6
0.7
0.8
0.9
1.0
ωc/ω

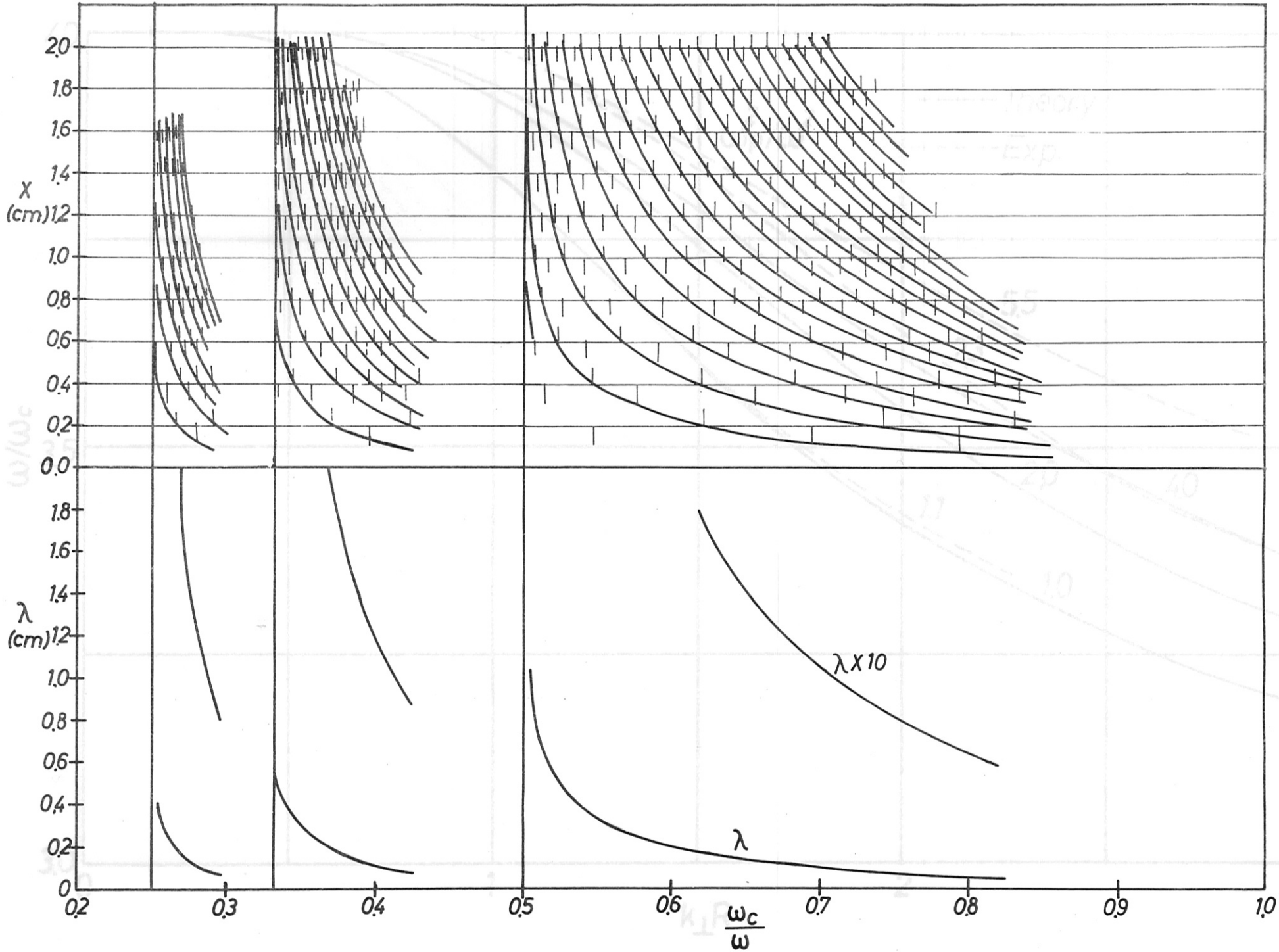
2.0
1.8
1.6
1.4
χ
(cm) 1.2
1.0
0.8
0.6
0.4
0.2
0.0
1.8
1.6
1.4
λ
(cm) 1.2
1.0
0.8
0.6
0.4
0.2
0
λ X 10
λ
0.2
0.3
0.4
0.5
0.6
0.7
0.8
0.9
1.0
ωc/ω

Figure 10

Figure 11a

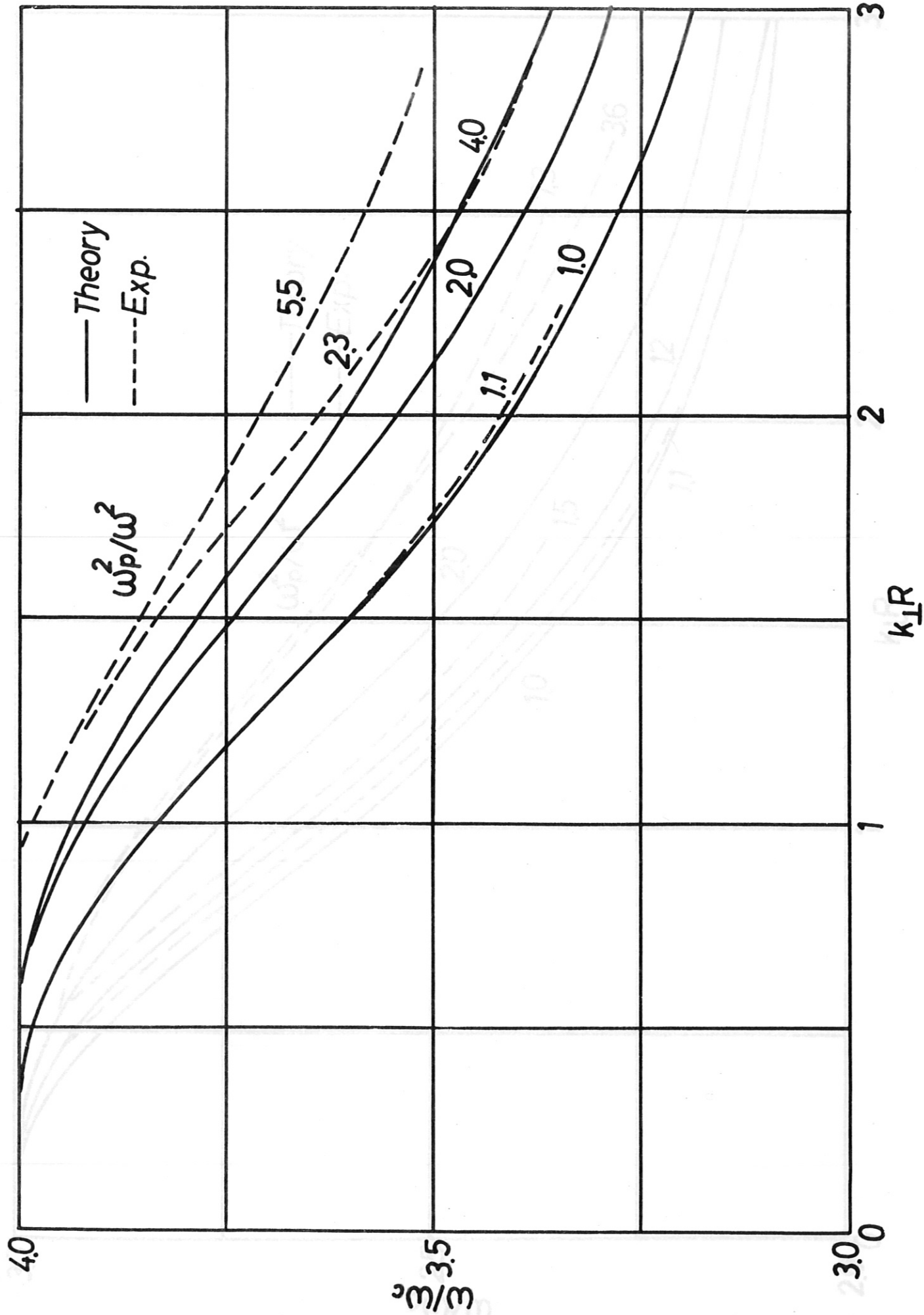
Theory
Exp.
ω_p^2/ω^2
5.5
4.0
2.3
2.0
1.1
1.0
$k_\perp R$
0
1
2
3
4.0
3.5
3.0
ω/ω_c

Figure 11b

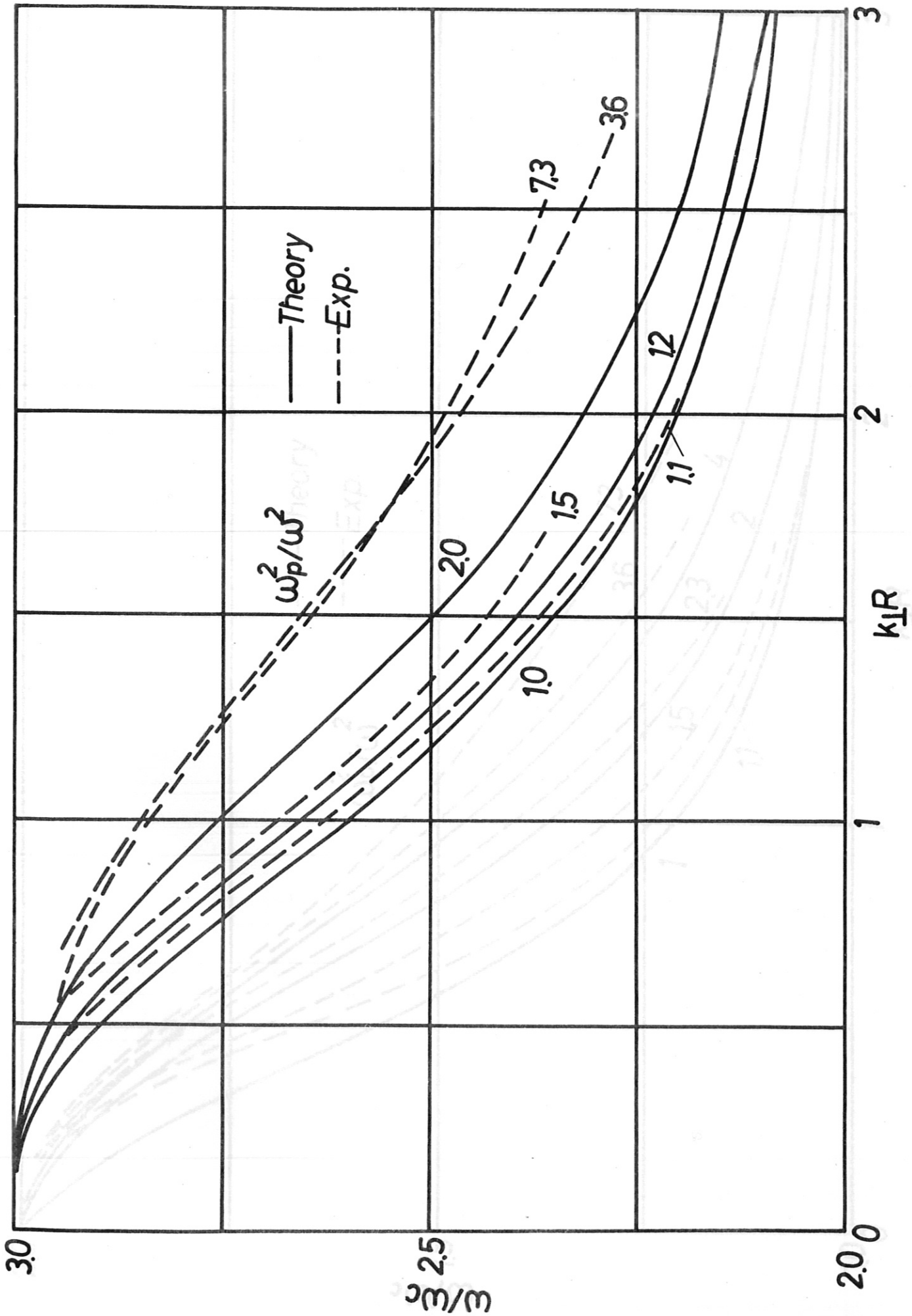
Theory
Exp.
ω_p^2/ω^2
3.6
7.3
12
2.0
1.5
1.1
1.0
k_1R
0
1
2
3
3.0
2.5
2.0
ω/ω_p

Figure 11c

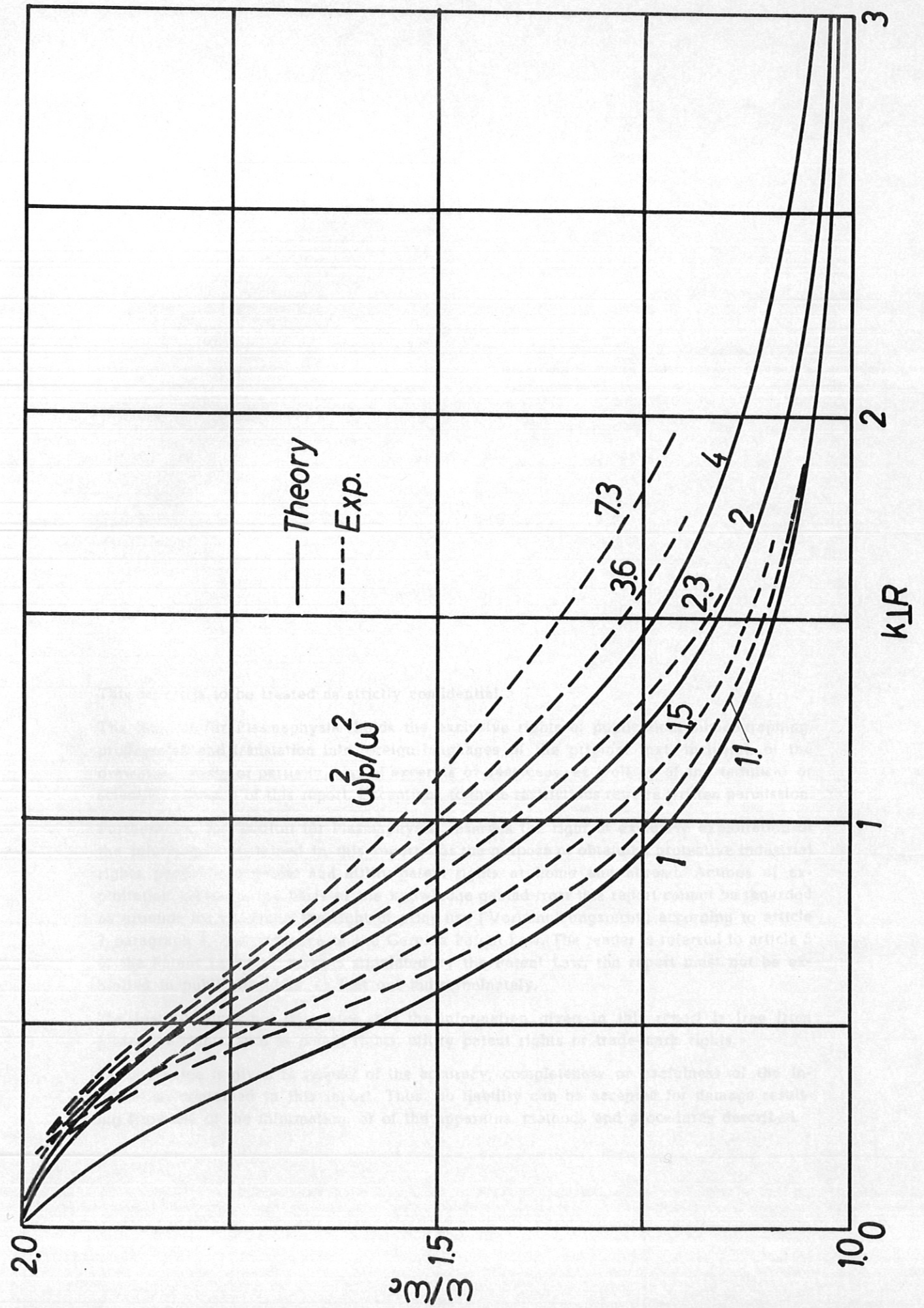
Theory
Exp.
ω_p^2/ω^2
7.3
3.6
2.3
1.5
1.1
4
2
1
2.0
1.5
1.0
0
1
2
3
$k_\perp R$